ELSEVIER

Biochimica et Biophysica Acta 1418 (1999) 268–284

BIOCHIMICA ET BIOPHYSICA ACTA
BBA

Analysis of calcium-induced calcium release in cardiac sarcoplasmic reticulum vesicles using models derived from single-channel data

Alexandra Zahradníková *, Ivan Zahradník

Institute of Molecular Physiology and Genetics, Slovak Academy of Sciences, Vlárska 5, 833 34 Bratislava, Slovak Republic

Received 9 December 1998; received in revised form 12 February 1999; accepted 22 February 1999

Abstract

The planar lipid bilayer and vesicle release experiments are two alternative approaches used to study the function of the ryanodine receptor (RyR) channel at the subcellular level. In this work, we combine models of gating (Zahradníková and Zahradník, Biophys. J. 71 (1996) 2996–3012) and permeation (Tinker et al., J. Gen. Physiol. 100 (1992) 495–517) of the cardiac RyR channel to simulate calcium release experiments on sarcoplasmic reticulum vesicles. The resulting model and real experimental data agreed well within the experimental scatter, confirming indistinguishable properties of the RyRC in the vesicle preparation and in the planar lipid bilayer. The previously observed differences in calcium dependencies of the release and the gating processes can be explained by binding of calcium within the RyRC conducting pore. A novel method of analysis of calcium dependence of calcium release was developed and tested. Three gating models of the RyRC, showing, respectively, an increase, no change, and a decrease in calcium sensitivity over time, were compared. The described method of analysis enabled determination of temporal changes in calcium sensitivity, giving potential for detection of the adaptation/inactivation phenomena of the RyRC in both vesicle and in situ release experiments.

Keywords: Calcium release; Ryanodine receptor; Permeation; Gating; Modeling; Cardiac muscle

1. Introduction

Three principal approaches, differing in their digression from in vivo conditions, were used in studies of the machinery providing for calcium release from intracellular stores in heart muscle: (1) measurements of calcium transients in skinned or living cells [1–4] with minimal perturbation of in vivo conditions; (2) measurements of $^{45}Ca^{2+}$ release from isolated vesicles of sarcoplasmic reticulum [5–9] in which native membrane composition is retained; or (3) measurements of single-channel activity of release channels incorporated into planar lipid bilayers [6,8,10–14]. Reconstitution of the channels into the artificial environment of the bilayer provides unrivaled time resolution and exceptional control of the experimental conditions, but the physiological relevance of the results has been questioned.

Bilayer experiments aided with rapid changes of Ca^{2+} in the vicinity of the single cardiac ryanodine receptor channel (RyRC) have revealed temporal changes in the channel activity [11,15–20], termed adaptation [15], which are accompanied by changes in the distribution of modes of channel activity [21,14]. The techniques for rapid Ca^{2+} concentration changes in the vicinity of a bilayer membrane still

* Corresponding author. Fax: +421 (7) 5477-3666; E-mail: umfgzahr@kramare.savba.sk

0005-2736/99/$ – see front matter
PII: S0005-2736(99)00036-X

suffer from technical limitations. Therefore, there is a continuing dispute whether the decrease in the RyRC sensitivity to Ca^{2+}, observed within seconds after channel activation [15], is a genuine property of the cardiac ryanodine receptor or a technical artifact [22–24]. The problem could not be addressed by measuring calcium release using stopped-flow techniques for the lack of a method of data analysis capable of resolving temporal changes in calcium sensitivity of release.

Another unresolved problem is the Ca^{2+} dependence of cardiac RyRC activity at high Ca^{2+} concentrations. In skinned cardiac Purkinje cells, Fabiato [1] has found that the extent of calcium release is a bell-shaped function of the free cytosolic calcium concentration. Also in isolated cardiac SR vesicles, the measured rate of passive $^{45}Ca^{2+}$ efflux was a bell-shaped function of the extravesicular calcium concentration [6–9], although the half-inhibiting Ca^{2+} concentration was an order of magnitude higher than that reported by Fabiato [1] in skinned myocytes. These observations were interpreted as evidence for a direct inhibitory action of calcium ions on cardiac Ca release via reduction of the open probability of the channel (Ca-dependent inactivation). However, this interpretation is at odds with the results of most single-channel experiments, in which the activity of cardiac calcium release channels was found to be inactivated, under similar conditions, by *cis* (cytosolic) calcium either at extremely high Ca^{2+} concentrations [13], or not at all [8,11,12]. It was attempted to avoid these contradictions by postulating that a hypothetical diffusible factor – supposedly lost during incorporation of the RyRC into the bilayer [8], or by treatment of the RyR channel with CHAPS during protein purification, or by high concentrations of Cs^{+} [13] – mediates calcium-induced inactivation.

Recent development in understanding of RyRC gating and permeation provides the means to interpret single-channel activity of the channel and the kinetics of macroscopic release on common grounds. In this work, we show how the mathematical descriptions of channel open probability and ion fluxes through the open pore of the channel can be combined to provide a unified model of calcium release. Using this approach, we will explore a hypothesis integrating the experimental observations obtained with the techniques of planar lipid bilayers and vesicle release experiments. According to this hypothesis, the experimentally observed time- and calcium-dependence of calcium release arise from the modal behavior of the release channel, and from the permeation properties of its conducting pore. This work is based on mathematical modeling with the use of the minimal gating model of cardiac RyRC developed by us [25], and with the use of the single ion permeation model of this channel described by Tinker et al. [26].

We introduce a new method for quantitative analysis of the Ca release data and, using three different models of RyR gating, we demonstrate that it can reliably detect temporal changes in the sensitivity of the RyRC to the activating ligands.

2. Materials and methods

Simulations of the calcium release fluxes from SR vesicles via RyRC were performed with a set of differential equations describing the three processes involved: the channel gating, the ion fluxes through the open channel, and the material balance of the system.

(1) Gating of the cardiac Ca release channel was described by a six-state scheme illustrated in Fig. 1A, which was shown to be the minimal gating scheme of the RyRC [25]. The rate constants of the model were that same as in [25]. The model predicts a transient increase in the channel open probability upon binding of a single Ca^{2+} ion to the activation site (Fig. 1B). It should be noted that the decrease of the channel activity in time is not a consequence of another Ca^{2+} ion binding to a site on the channel, occupation of which would cause channel transitions to the inactivated state. Rather, inactivation involves spontaneous, slow, kinetically controlled transitions of the channel to modes having a lower open probability than the mode in which the channel resides during activation. Modeling was performed in the environment of the Mathematica program (Version 2.2, Wolfram Research, USA) running on a Pentium computer as described previously [25]. The time courses of open probabilities after application of a step change in *cis* calcium concentration, such as the example in Fig. 1B, were calculated by solving a

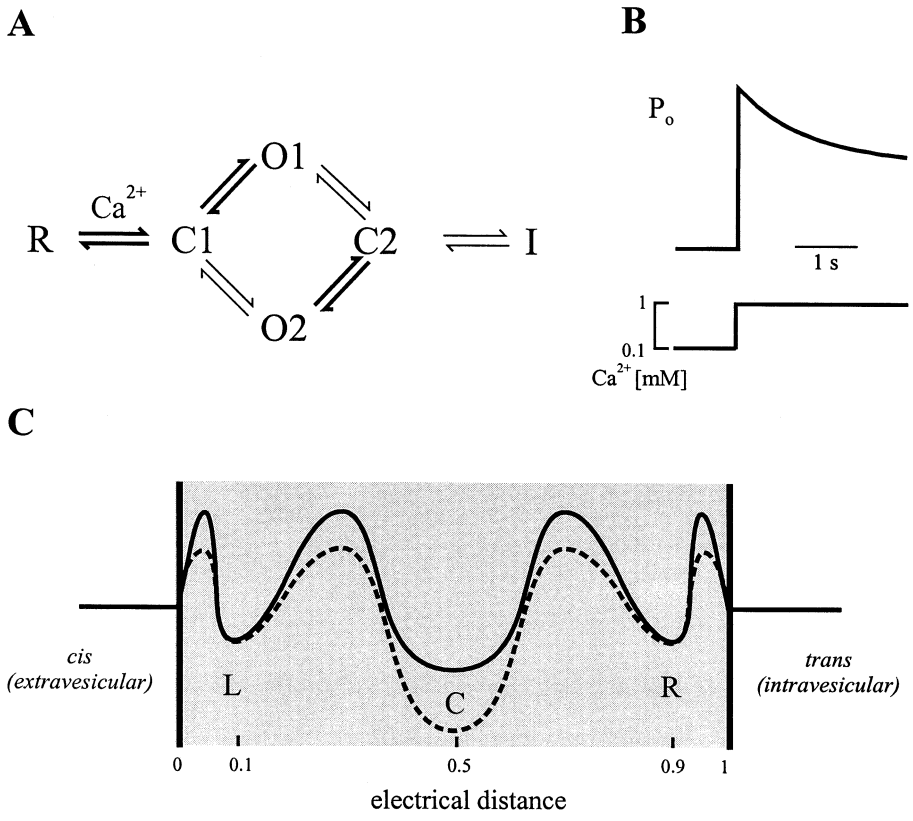

Fig. 1. The gating and permeation schemes of the RyRC. (A) The minimal gating model according to Zahradníková and Zahradník [25]: R, resting state; C1 and C2, closed states; O1 and O2, open states, I, inactivated state. Thick arrows denote fast transitions and thin arrows denote slow transitions. (B) Illustration of the transient response of the gating model to a step change of Ca^{2+} from 0.1 to 1 μM. (C) Schematic diagram of the energy profile of the RyR channel pore according to Tinker et al. [26]. The relative energies of channel wells and barriers are approximately shown (solid line, monovalent cations; dashed line, divalent cations).

system of ordinary differential equations of channel kinetics, using the set of rate constants estimated in our previous work [25]. The apparent activation constant $K_a^{app}(t)$ of the channel open probability $P_o(t)$ at the time t after a step change of Ca^{2+} was estimated by fitting the dose–response equation to the calculated open probabilities at a given time.

(2) The single-ion channel pore model [26] depicted in Fig. 1C was solved in Mathematica running on a Pentium computer, using a set of steady-state equations for state probabilities as described in Cooper et al. [27], allowing for a maximum of four different permeant ions. The model was applied here to calculate the RyR single-channel conductances (simulated bilayer experiments), and the flux of $^{45}Ca^{2+}$ through the open RyR channels (simulated vesicle experiments).

(3) The time course of $^{45}Ca^{2+}$ release from vesicles was solved in Mathematica running on IBM RISC/6000 machine. The differential equations for channel gating [25] were combined with Eqs. 1 and 2 for non-steady state flux through the open pore of the single-ion channel [27]. These equations were derived assuming that in the closed channel no transitions of ions between channel pore wells can occur.

$$\frac{dW_{M_i}(t)}{dt} = P_o(t)\cdot\left(-W_{M_i}(t)\cdot\sum_{j\neq i}k_{M_{ij}} + \sum_{j\neq i}\left(k_{M_{ji}}\cdot W_{M_j}(t)\right) + k_{M_{Ei}}\, W_E(t)\, [M_i](t)\right) \quad (1)$$

$$\frac{dW_E(t)}{dt} = P_o(t)\cdot\left(-W_E(t)\sum_i\left(k_{M_{Ei}}[M_i](t)\right) + \sum_i\left(k_{M_{iE}}\, W_{M_i}(t)\right)\right) \quad (2)$$

The indices i,j denote the position of the ion in one of the three wells (R, C, L); $[M_i](t)$ is the free concentration of ion M in the compartment neighboring with the well i, i.e. intravesicular compartment (right well) or extravesicular compartment (left well); $k_{M_{ij}}$ are the rate constants of the transition of the ion M from the well i to the well j or into/out of the channel ($k_{M_{CE}} = k_{M_{EC}} = 0$ by definition); $W_{M_i}(t)$ is the probability of the channel pore energy well i to be occupied by the ion M, $W_E(t)$ is the probability of all the channel energy wells being empty.

The equations of material balance (Eqs. 3–6); Ca^{2+} and $^{45}Ca^{2+}$ were considered different species) were solved for the transport of ions between the compartments and for the complexation of calcium by the chelator EGTA (ethylene glycol *bis*-β-aminoethyl ether-*N*,*N*,*N*′,*N*′-tetraacetic acid). The rate constants k_{on} and k_{off} for binding of calcium to EGTA were taken from Smith et al. [28]. Binding of other ions by EGTA is weak and was not considered. The initial conditions for EGTA complexation were solved based on the dissociation constants reported by Smith and Miller [29]. In simulations where the extravesicular compartment was assumed to behave as an infinite sink, i.e. the extravesicular concentration of $^{45}Ca^{2+}$ was not influenced by the efflux, the right sides of Eqs. 3–6 were set to zero.

$$\frac{d[M_R](t)}{dt} = P_o(t)\frac{n}{V_R}(k_{M_{RE}}\ W_{M_R}(t) - k_{M_{ER}}\ W_E(t)[M_R](t)) \quad (3)$$

$$\frac{d[M_L](t)}{dt} = -\frac{V_R}{V_L}\frac{d[M_R](t)}{dt} - k_{on}[\mathrm{EGTA}](t).[M_L](t) + k_{off}\ [M.\mathrm{EGTA}](t) \quad (4)$$

$$\frac{d[\mathrm{EGTA}](t)}{dt} = -k_{on}\ [\mathrm{EGTA}](t)\sum_{m}[M_L](t) + k_{off}\sum_{m}[M.\mathrm{EGTA}](t) \quad (5)$$

$$\frac{d[M.\mathrm{EGTA}](t)}{dt} = k_{on}\ [\mathrm{EGTA}](t).[M_L](t) - k_{off}\ [M.\mathrm{EGTA}](t). \quad (6)$$

Here, n is the total number of RyR channels, V_R is the total vesicular volume, V_L is the total extravesicular volume.

The buffering of intravesicular calcium by calsequestrin was considered to be instantaneous, and the free calcium concentration was calculated as in [30]:

$$[Ca^{2+}] = \frac{1}{1 + \frac{K_D c_{csq}}{(K_D + c_{Ca})^2}} \quad (7)$$

where $[Ca^{2+}]$ is the intravesicular concentration of free Ca^{2+}, $K_D = 0.5$ mM [31] is the dissociation constant for Ca binding to calsequestrin binding sites, c_{csq} is the concentration of these sites, and c_{Ca} is the total intravesicular calcium concentration.

In the case when the effect of open probability inhibition by calcium on release was considered, the inhibition was assumed to be independent of activation, and P_o in Eqs. 1–3 was then multiplied by the inhibitory dose–response function.

To inspect $^{45}Ca^{2+}$ efflux without contribution of the channel time dependent behavior on the kinetics of release, the open probability P_o in Eqs. 1–3 was calculated using the dose–responses of activation [25] for the peak or the steady-state open probability.

For testing the performance of the procedure for determination of the sensitivity of the channel to activation by Ca^{2+} as a function of time, three models differing in the time dependence of K_a were considered.

As Model 1, a representative of models in which K_a decreases as a function of time, we used the minimal gating model as described above. The time constant of K_a equilibration is ~1 s in the activating Ca^{2+} range of about 1–10 μM.

As Model 2, a representative of models in which K_a does not change in time, we used a gating model with instantaneous activation to

$$P_o = \frac{Ca^{2+}}{Ca^{2+} + K_a}$$

and the value of $K_a = 2.4$ μM.

As Model 3, a representative of the models in which K_a increases as a function of time, we used a gating model with the following calcium- and time-dependence of open probability:

$$P_o = \frac{[Ca^{2+}]^n}{[Ca^{2+}]^n + (K_a(t))^n},$$

$$K_a(t) = K_a(0) - \Delta_{K_a}\left(1 - e^{-\frac{t}{\tau_{Ca}}}\right), \quad (8)$$

The parameter values were: $K_a(0) = 0.3$ μM, $K_a(\infty) = 2$ μM, $\Delta_{K_a} = K_a(\infty) - K_a(0)$, $\tau_{Ca} = 1$ s; $n = 4$. This model is approximately equivalent to the model of Keizer and Levine [32].

The rate of release was estimated from the time courses of intravesicular $^{45}Ca^{2+}$ concentration using three procedures, mimicking real experimental techniques: (1) the initial release rate method – as the slope of the release curve calculated with 50 ms time resolution (or 1 ms, to avoid the low sampling rate errors); (2) the cumulative release method – as the amount of calcium released within 5 s; and (3) the half-time method – as the reciprocal value of the release half-time. The values of efflux rates are given in relative units, as the channel density in the release experiments is not known.

3. Results

3.1. Calcium dependence of the RyRC open probability

The calculated calcium dependence of the steady-state open probabilities is compared to the experimental data of Chu et al. [8], Györke et al. [11], and Laver et al. [13] in Fig. 2. All these data were obtained in the absence of Mg^{2+} and ATP, and using Cs^+ as the charge carrier. It is obvious that the theoretical calcium dependence of the steady-state curve (solid line) is a good approximation of the measured values up to 1 mM Ca^{2+} concentration. Approximation of all published data in the range below 1 mM with a dose–response function provided the activation constant $K_a = 1.22 \pm 0.21$ μM and the slope $n_H = 1.16 \pm 0.20$. These values are almost identical to the theoretical predictions of the model of 0.97

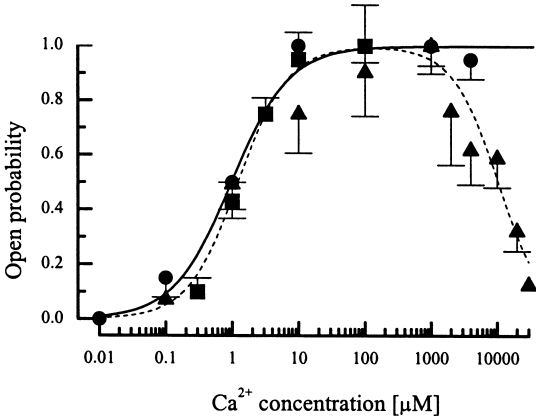

Fig. 2. Calcium dependence of the open probability of the RyR channel. The experimental data are replotted as solid symbols with corresponding error bars (circles, Chu et al. [8]; squares, Györke et al. [11]; triangles, Laver et al. [13]). Dashed line, a fit to all the experimental data (with the product of the activatory and inhibitory dose–response functions). Solid line, theoretical steady-state open probability as a function of Ca^{2+} concentration. Both the calculated and the experimental data are normalized for comparative purposes.

μM and 1.0 for K_a and n_H, respectively. For calcium concentrations above 1 mM, only few data are available. The results of Laver et al. [13] differ from the other two reports by observation of a decline in P_o. Inclusion of these data into the fit did not change the activation parameters. Additionally, it provided the inhibition parameters $K_i = 10.4 \pm 1.3$ mM and $n_i = 1.26 \pm 0.20$ for the calcium dependent open probability inhibition (dashed line), close to the reported values of $K_i = 15$ mM and $n_i = 1.7$ [13]. The contribution of the calcium-dependent inactivation to the open probability is less than 10%, i.e. well within the experimental error, up to 2 mM *cis* Ca^{2+}. It can be concluded that the minimal gating model approximates the experimental data very well and can be applied up to the millimolar range of activating Ca^{2+}.

3.2. Ion permeation through the RyR channel

Our implementation of the permeation model of Tinker et al. [26] was tested by calculation of the single-channel current–voltage curves for the mixed solutions of K^+ with Ca^{2+} or Ba^{2+}, of the limiting conductances, and of K_D constants for monovalent and divalent ions. The calculated values (Table 1) were almost identical to the original data published

Table 1
Conduction parameters of the ryanodine receptor channel for monovalent and divalent cations

Ion	K_D (mM)			g_{max} (pS)			g_{210} (pS)			$P_{M^{z+}}/P_{K^+}$		
Cs^+	**34**	*34*	(34)	**644**	*621*	(588)	**555**	*500*	(460)	**0.52**	*0.50*	(0.61)
K^+	**23**	*23*	(20)	**852**	*831*	(900)	**767**	*712*	(723)	**1.00**	*1.00*	(1.00)
Na^+	**15**	*15*	(18)	**539**	*530*	(516)	**503**	*481*	(446)	**1.00**	*1.02*	(1.15)
Li^+	**6.8**	*7.4*	(9.1)	**245**	*244*	(248)	**237**	*234*	(215)	**1.00**	*1.05*	(0.99)
$Tris^+$	**6.9**	*5.4*	–	**24**	*25*	–	**24**	*24*	(17)	**0.14**	*0.20*	(0.22)
Ca^{2+}	**0.121**	*0.116*	–	**186**	–	–	**109**[a]	*94*[a]	(94)[a]	**6.06**	*7.15*	(6.50)
Ba^{2+}	**0.172**	*0.165*	–	**205**	–	–	**205**	*191*	(199)	**5.29**	*5.28*	(5.80)
Sr^{2+}	**0.127**	*0.123*	–	**195**	–	–	**195**	*181*	(183)	**6.06**	*5.88*	(6.70)
Mg^{2+}	**0.090**	*0.086*	–	**138**	–	–	**137**	*128*	–	**6.05**	*6.93*	(5.90)

The numbers in boldface are solutions of our implementation of the permeation model; the numbers in italics are the theoretical calculations of Tinker et al. [26]; and the numbers in parentheses are their experimental data. K_D, the binding constant of the ion to the channel pore; g_{max}, the limiting conductance; g_{210}, conductance in symmetrical 210 mM solution of the respective chloride salt; P, the ionic permeabilities.

[a]The figures given are obtained for ionic conditions of 60 mM Ca^{2+} *trans*, 125 mM Tris *cis* [26].

by Tinker et al. [26]. The small differences might be due to the higher (30-digit) numerical precision of the Mathematica program used here.

Calculations of the single-channel current amplitudes, *I–V* curves, and conductances to be used for simulation of bilayer experiments were performed for 250 mM Cs methanesulfonate and variable $CaCl_2$ in the *cis* compartment, and 50 mM Cs methanesulfonate and 3 μM Ca^{2+} in the *trans* compartment, to match the experimental conditions used in the only report [8] that directly compares results of the single-channel and release experiments. The amplitudes of single-channel currents were calculated for the voltage range of −60 to +60 mV at different activating *cis* Ca^{2+} concentrations ranging from 0.1 μM to 100 mM. From these data, the conductances of the RyR channel at different levels of *cis* Ca^{2+} were calculated as the slope of the respective *I–V* curves in the linear range from −60 to +20 mV and normalized to the value at 1 μM *cis* Ca^{2+}. The calcium dependence of the normalized channel conductance, predicted by the pore model (i.e. not fitted to the experimental data), is given in Fig. 3 (upper panel, solid line). The simulated RyR open channel conductance hyperbolically decreases with Ca^{2+} with $K_i = 2.83$ mM and $n_H = 1.0$. The predictions of the model, which was derived from sheep cardiac RyRC data [26], is in good correspondence with the experimental data reported for the canine channel ($K_i = 5.4$ mM and $n_H = 0.8$; [8]), replotted in Fig. 3 (upper panel).

3.3. Simulations of $^{45}Ca^{2+}$ efflux

The currents depicted in the upper panel of Fig. 3 are mostly carried by Cs^+ ions. The simulation approach allows calculating the ionic currents and unidirectional fluxes through the open RyRC for Ca^{2+} ions as well. We have used slightly different ionic conditions for this calculation, in order to compare these data with the results of release flux experiments. Ionic conditions were chosen according to those employed in the report of Chu et al. [8] (in mmol/l): 100 KCl, 20 K_2HEPES, 0.1 $MgCl_2$, 5 K_2EGTA, variable $CaCl_2$ for the extravesicular, and 100 KCl, 20 K_2HEPES, 2 $CaCl_2$ for the intravesicular compartment. The calcium current through a single RyRC at 0 mV is depicted in Fig. 3 (lower panel) as a solid line. The initial amplitude of I_{Ca} carried by 2 mM Ca^{2+} ions was −2.2 pA. As the concentration of Ca^{2+} in the *cis* compartment increased, the current decreased and reversed sign at *cis* $Ca^{2+} = 2$ mM. On the other hand, the unidirectional efflux of Ca^{2+} from the *trans* compartment decreased sigmoidally, starting from the initial 2.2 pA, with a K_i of 3.26 mM (the dashed line in Fig. 3, lower panel).

The published experimental data on calcium dependence of calcium release from cardiac SR vesicles [6–9] are shown in Fig. 4. To allow for a direct comparison, only data obtained in the absence of ATP and utilizing passive $^{45}Ca^{2+}$ loading were included.

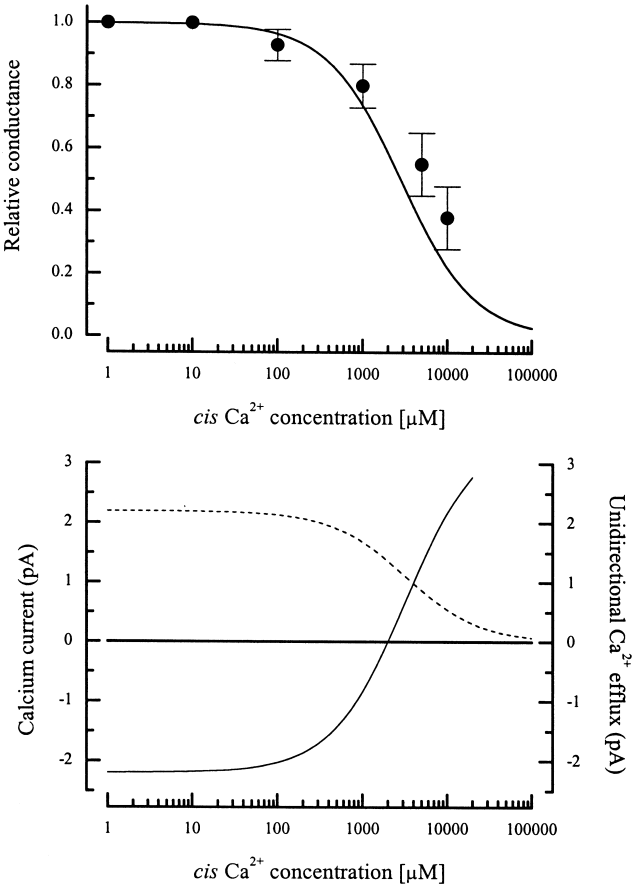

Fig. 3. Calcium dependence of the RyRC single-channel conductance. Upper panel: theoretical single channel conductance, expressed relative to that in the absence of Ca^{2+}, plotted as a function of *cis* Ca^{2+} concentration (solid line). The data reported by Chu et al. [8] are plotted as solid circles with error bars. Lower panel: theoretical single channel current at 0 mV under ionic conditions used in the release experiments (solid line), compared with the unidirectional efflux of Ca^{2+} ions through the open channel (in units of pA) from the *trans* compartment, which corresponded to the luminal side of the channel (dashed line).

The data are significantly scattered, despite the fact that experiments were performed under relatively similar conditions. The first question was, what is the relationship between the experimental data and the theoretical predictions, and the second, whether the model can explain the differences between the experiments.

To answer the first question, calculations of $^{45}Ca^{2+}$ efflux curves were performed first using idealized conditions, namely: the approximation that the extravesicular compartment behaves as an infinite sink; time resolution of 1 ms; and the initial rate method of analysis. Ionic conditions were again chosen according to those employed in the report of Chu et al. [8] (in mmol/l): 100 KCl, 20 K_2HEPES, 0.1 $MgCl_2$, 5 K_2EGTA, variable $CaCl_2$ for the extravesicular, and 100 KCl, 20 K_2HEPES, 2 $^{45}CaCl_2$ for the intravesicular compartment. Interactions of Ca^{2+}, $^{45}Ca^{2+}$, K^+, and Mg^{2+} with the channel pore were taken into account. The time course of $^{45}Ca^{2+}$ efflux was calculated for extravesicular Ca^{2+} concentrations from 0.001 μM to 100 mM (at least three points per decade), and for a channel density (1 nmol RyR per 1 l of intravesicular volume) providing a half-time of 0.3 s at the Ca^{2+} concentrations (10–100 μM) that evoked the fastest release. This value is well in the range of the experimentally observed efflux rates. The results are shown normalized to the maximal rate of release in Fig. 4A.

In the Ca^{2+} concentration range from 0.001 to 100 μM, the relative release rate estimated from these simulated data increases as a sigmoidal function of log [Ca^{2+}], following the calcium dependence of the channel peak open probability (for details see [25]), and gives 50% activation of release at 4.8 μM extravesicular Ca^{2+}. The experimental release data, although of similar shape, are mostly to the left of the theoretical predictions. At Ca^{2+} concentrations higher than 100 μM, the relative release rates estimated from the simulated data decline, following the calcium dependence of the channel permeation (see Fig. 3, top panel), with half inhibition of release at 1.8 mM Ca^{2+}. In the high calcium concentration range, the experimental release rate data are mostly to the left of the simulated data. Although the extent of errors was not reported with the experimental data, the decline of release is obvious. The decrease of the simulated release rate at high Ca^{2+} is fully due to a decrease in the efflux through the open channel, as in the model neither the peak nor the steady-state open probability decline at high calcium concentrations.

3.4. Analysis of release experiments

Although the overall reported experimental conditions for the data given in Fig. 4A were similar, several experimental details and the methods of anal-

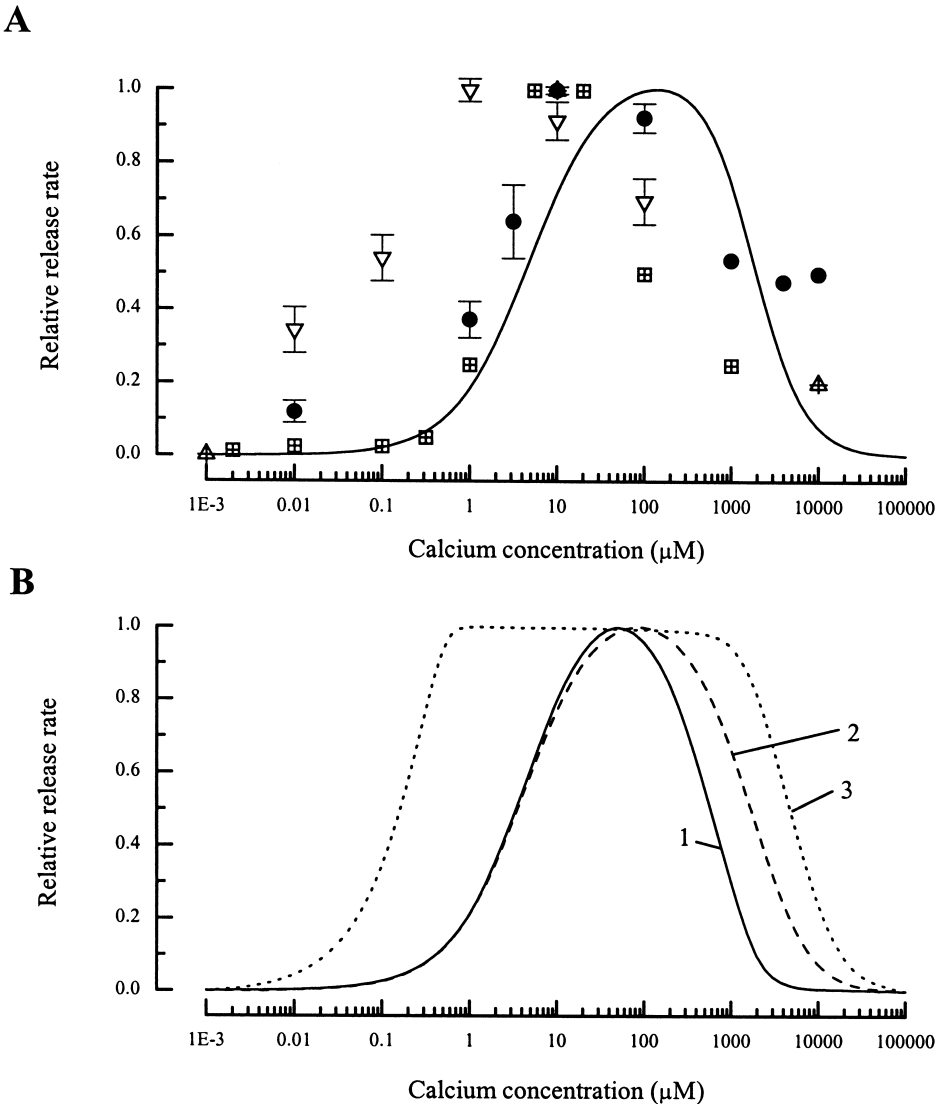

Fig. 4. Relative rate of calcium release from SR vesicles at different extravesicular Ca^{2+} concentrations. (A) The reported experimental data with their standard errors (if reported) are plotted as: solid circles, Chu et al. [8]; open triangles, Mészáros et al. [9]; crossed triangles, Rousseau et al. [6]; and crossed squares, Meissner and Henderson [7]. The 'true' initial rate of $^{45}Ca^{2+}$ release predicted by the model, normalized to that at optimal Ca^{2+} concentration is plotted as solid line. (B) Simulations of the Ca^{2+} dependence of the release rate for different experimental conditions: curve 1, using the half-time method, $^{45}Ca^{2+}$ loading of 200 μM, and infinite capacity of the extravesicular sink; curve 2, using the initial rate method with 50 ms time resolution, $^{45}Ca^{2+}$ loading of 2 mM, and infinite capacity of the extravesicular sink; and curve 3, using the cumulative 5 s release technique, $^{45}Ca^{2+}$ loading of 2 mM, 250 μM extravesicular EGTA and vesicle dilution 1:50.

ysis were different. The differences include: the buffering capacity of the extravesicular sink for the released calcium (EGTA concentration and dilution of vesicles), intravesicular calcium concentration (the extent of $^{45}Ca^{2+}$ loading), and the measure used for the release rate estimation (either the initial release rate, or the amount of $^{45}Ca^{2+}$ released per 5 s, or the reciprocal half-time of release). The approach of simulation is the ideal one to study the contribution of these factors to the experimental results. This might also help to understand, under which conditions the experimental errors can be minimized. Thus, to answer the second question mentioned above, we have set the parameters of the model to correspond to the conditions used in the reports of Meissner and Henderson [7], Chu et al. [8], or Mészáros et al. [9]. The

resulting consequences for the calcium dependence of release are shown in Fig. 4B for comparison. It is to note that the resulting simulations are not fits to the experimental data, but they rather describe calcium release at a specific set of conditions.

The simulated curve for the half-time method, with infinite sink approximation and $^{45}Ca^{2+}$ loading of 200 μM (corresponding to [7]), is plotted in Fig. 4B as curve 1. The relative release rate peaks at a lower Ca^{2+} concentration than does the theoretical curve, with half activation occurring at 3.8 μM Ca^{2+}, and half inhibition at 0.55 mM. The simulated curve for the initial rate method, with infinite sink approximation and $^{45}Ca^{2+}$ loading of 2 mM (corresponding to [8]), and 50 ms sampling period is shown as curve 2. In this case, 50% activation occurs at 3.8 μM Ca^{2+} and 50% inhibition at 1.6 mM Ca^{2+}. A simulation using 250 μM EGTA, vesicle dilution 1:50, 2 mM $^{45}Ca^{2+}$, and release rate defined as $^{45}Ca^{2+}$ released per 5 s (corresponding to [9]) is shown by curve 3. The ascending arm of the curve is substantially shifted to the left, providing 50% activation at 0.14 μM. The descending arm gives increased half inhibition value of 4.7 mM Ca^{2+}. This method provides estimate of the half activation of release which is in close correspondence with the reported data [9]. However, as it also shifts the declining part of the curve to the right, the use of the method of cumulative 5 s release cannot explain the reported partial reduction of release observed already at 100 μM Ca^{2+} [9].

For deeper insight into the effect of experimental conditions and methods of analysis on the relative magnitude of the K_a and K_i values, we have performed simulations for combinations of the following conditions: intravesicular Ca^{2+} of 0.2, 2.0, or 20 mM; the extravesicular sink either ideal or of 250 μM EGTA and vesicle dilution of 1:50; and the three above-mentioned methods of analysis. The gating model (Fig. 1) predicts that after rapid activation, the channel undergoes slow inactivation accompanied by a shift in the apparent K_a from 4.8 to 1.0 μM Ca^{2+}. To account for the non-stationarity of K_a, the K_a values were normalized to the prediction of the model for the time of their determination (i.e. 50 ms, 5 s, and the half-time at $Ca^{2+} = K_a$ for the three methods, respectively). The K_i values were normalized to the values obtained at the respective intravesicular calcium concentrations with the initial rate method and 1 ms resolution, which was considered to be error-free. The results, plotted in Fig. 5, confirm that the initial release rate method provides the best estimates of the binding constants. However, for any of the employed methods, the values of K_a tend to be underestimated, especially at high release rates and finite extravesicular sink. The differences are most apparent for the cumulative 5-s method,

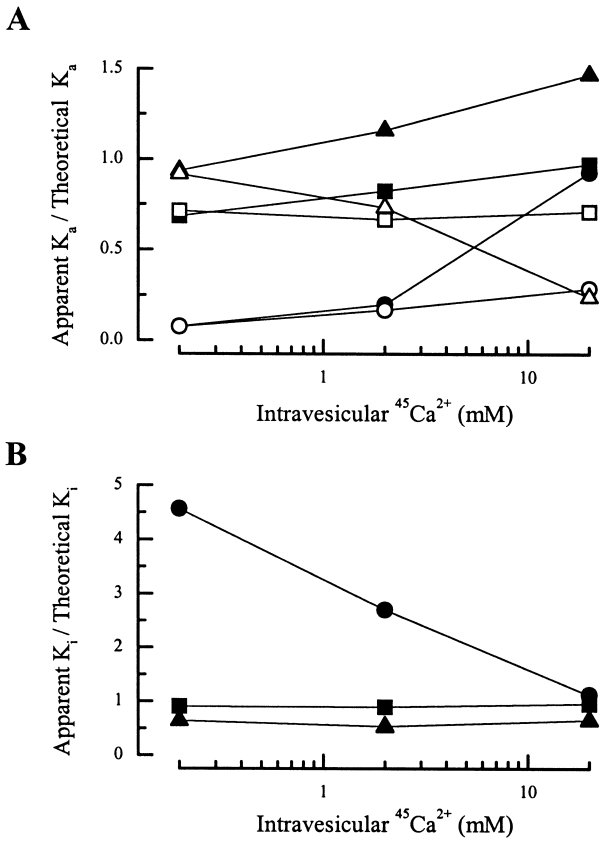

Fig. 5. The effect of $^{45}Ca^{2+}$ loading on the estimation errors of the K_a and K_i values for different experimental conditions. (A) The apparent K_a normalized to their theoretical values at the time of determination, plotted as a function of intravesicular $^{45}Ca^{2+}$. Squares, circles, and triangles stay for the methods of initial rate, cumulative 5 s release, and reciprocal half-time, respectively. The solid symbols correspond to the calculations with infinite calcium buffering capacity of the extravesicular sink. The open symbols correspond to calculations with a reduced capacity of the extravesicular sink (250 μM EGTA and 1:50 vesicle dilution). (B) The values of apparent K_i, normalized to the theoretical values, plotted as a function of intravesicular Ca^{2+}. The symbols have the same meaning as in A. Note that the solid and open symbols cannot be distinguished, as the K_i values were independent of the properties of the extravesicular sink.

with the error reaching almost one order of magnitude. The half-time method tends to underestimate K_i, while the cumulative 5-s method tends to overestimate it. The K_i values are not dependent on the Ca^{2+} ion buffering capacity of the extravesicular sink.

Generally, from these simulations it can be concluded that the time resolution of the methods for release rate estimation significantly influences the estimated calcium dependence of release. Even the methods with the best time resolution, i.e. the half-time method and the initial rate method, provide systematic deviations from the expected values. This finding points to the importance of kinetic processes involved in the release of calcium, namely, the gating of the channel, and the depletion of the vesicles. The depletion effect will be minimized, if the loading of vesicles with calcium is substantially increased and if the rate of efflux is decreased. Then, the kinetics of the release will be controlled solely by the kinetics of the RyRC gating. Below we will describe a method of analysis of the time course of release, based on the above considerations, useful for estimation of a time-dependent change of the K_a from real experimental data.

3.5. Estimation of the K_a shift from the release experiments

To isolate the effects of channel gating on release from those caused by vesicle depletion, in the following simulations the half-time of efflux at the optimal Ca^{2+} concentration was reduced from 0.3 to 18 s by decreasing the relative channel density (the n/V_R ratio in Eq. 3). With this rate of release, more than 75% of $^{45}Ca^{2+}$ was retained in the vesicles after 5 s of release.

We have compared three gating models, differing in their time dependence of calcium sensitivity: Model 1 is characteristic by a predicted decrease in K_a as a function of time, as described in [25]. At the start of activation by an increase in Ca^{2+} concentration, all channels have a K_a of 4.75 μM, and they equilibrate with a calcium-dependent time constant into the steady state with $K_a = 0.97$ μM; Model 2 has a time-independent value of $K_a = 2.4$ μM; and Model 3 is characteristic by an increase in K_a as a function of time from the initial value of 0.3 μM to the equilibrium value of 2 μM.

The calcium dependence of release was determined for a set of times, t (0.05, 0.1, 0.2, 0.5, 1, 2, and 5 s), during which the channel relaxed from the peak of activity down to the steady-state level. The estimates of the apparent K_a of the channels at any given time were compared to the respective theoretical values. As the measure of the release rate at the time t, the calculated amount of calcium released from the vesicles during the period from starting release until time t was taken. This procedure is illustrated in Fig. 6, in which the calcium dependence of release rate is constructed for the time point $t = 1$ s.

For every studied period, the values obtained with

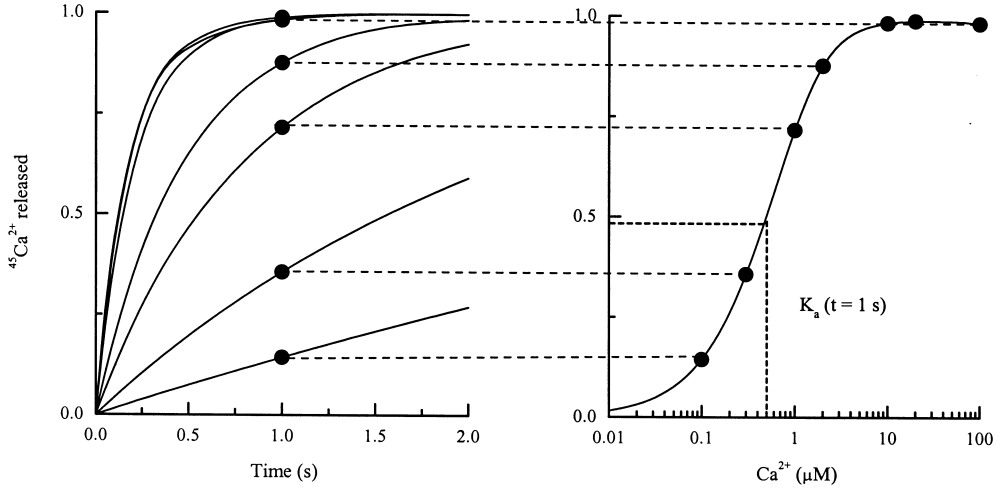

Fig. 6. The method of analysis. The proportion of $^{45}Ca^{2+}$ released at time t (left) is plotted against calcium concentration that induced release (right). The apparent K_{Ca} at time t is determined by fitting this calcium dependence with a dose–response curve.

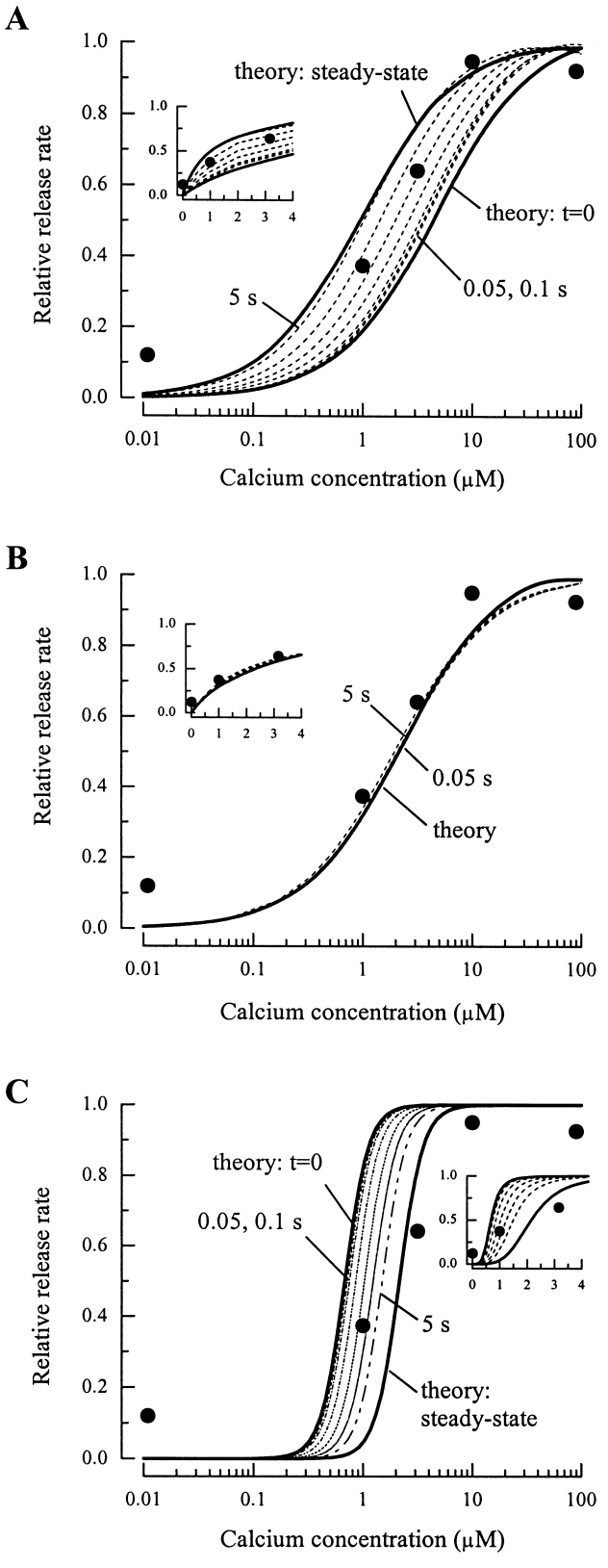

the above procedure were normalized. The results for Models 1, 2, and 3 are plotted in Fig. 7A–C, respectively. In Model 1, progressively longer time periods of Ca^{2+} efflux (lines labeled with the value of the period duration) provided the relative release rate curves shifting between the two theoretical limits from the right to the left. This shift resulted in an almost one order of magnitude difference in the estimated values of K_a for release activation. The interrelation between the equilibration of the channels and the shift of apparent K_a is documented in Fig. 7A by two curves for the approximation of time-invariant open probability. One represents the initial efflux rate for the channels at the peak open probability and the other stays for the channels at the steady-state open probability (all states are populated). It can be seen that the predicted calcium dependencies of release are of similar shape to the experimental data [8], and the curve at $t=1$ s is closest to the experimental data points.

In Model 2, the different time periods produced values of K_a that did not differ significantly from each other, nor from the theoretical value (Fig. 7B). The value of K_a in the model was chosen to be close to the experimentally obtained value [8], and therefore this model also describes the experimental release data adequately.

In Model 3, the calcium dependencies of the initial and steady-state open probabilities are similar to those predicted by the model of Keizer and Levine [32]. The shift of K_a values as a function of time, obtained from the release curves, was in agreement with the theoretical predictions, i.e. in the opposite direction as for Model 1. However, the value at 5 s of release was significantly lower than the predicted value (Fig. 7C). From Fig. 7C, it can also be seen that the slopes of the calcium dependence of release rate, predicted by Model 3, are much steeper than actually observed in the experiments [8], and there-

←

Fig. 7. The calcium dependence of calcium release at different times for the three employed models. The theoretical calcium dependencies of release at $t=0$ and at $t=\infty$ are plotted as thick lines. The calcium dependencies at different times (0.05, 0.1, 0.2, 0.5, 1, 2, and 5 s) are shown as thin lines and marked by the respective time. Insets: the calcium dependence of release replotted in liner scale. (A) Model 1. (B) Model 2. (C) Model 3. Solid circles are the experimental data from [8].

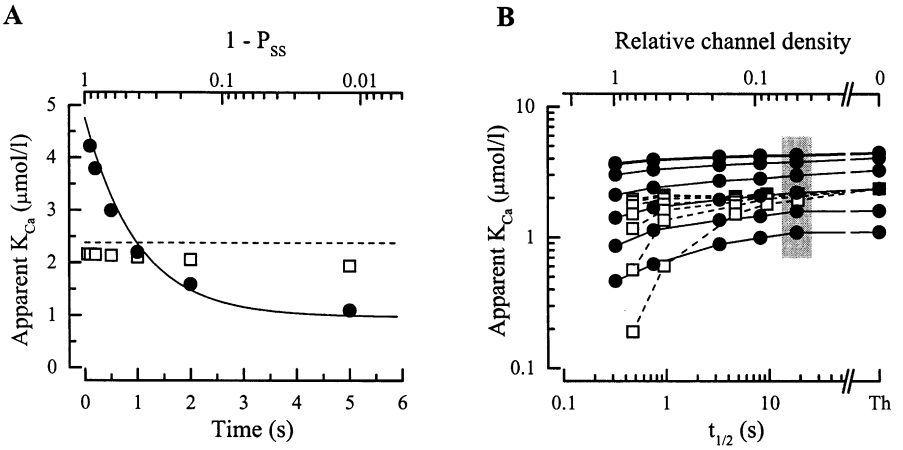

Fig. 8. The apparent calcium sensitivity of the release rate as a function of the time of determination. (A) The apparent K_a of the release rate of the model (solid circles) estimated at different times after starting the release (from the curves in Fig. 7A) is superimposed on the theoretical time course of the apparent K_a of the RyRC (solid line). The apparent K_a determined under identical conditions, but using Model 2 with a constant open probability equal to $P_{o,peak}$ is shown as open squares. The top axis ($1–P_{SS}$) – the proportion of channels that have not yet reached the steady-state. The relative channel density used for calculations was 0.05. (B) The effect of the rate of release on the apparent K_a determined at different times after commencement of release (top to bottom, solid circles stay for the times of 0.05, 0.1, 0.2, 0.5, 1, 2 and 5 s, respectively). The rate of release is expressed as the minimal half-time ($t_{1/2}$; lower axis), or as the relative channel density (top axis). Open squares show the apparent K_a values determined for Model 2. The data related to the part A of the figure are marked by gray background.

fore the experimental data cannot be adequately described by this model.

Altogether, Figs. 6 and 7 exemplify the method for evaluation of the time shifts in the channel affinity from experimental release data.

The relation between the apparent K_a and the proportion of channels that entered the steady-state (P_{SS}) during the time course of release is evaluated in Fig. 8A for the case of Model 1. The time course of the estimated apparent K_a reflects well the theoretical change in the apparent K_a of the channel during progression to the steady state. The correlation between the two estimates of K_a is very good ($r = 0.996$). For comparison, analogous result for Model 2 is also provided in Fig. 8A, to show that the artificial decrease of apparent K_a would not exceed 20%.

In real experiments, high efflux rates can corrupt the estimated calcium dependencies. The relationship between the values of release half-time $t_{1/2}$ at optimal [Ca^{2+}] (inversely proportional to channel density; upper axis) and the estimate of the apparent K_a is plotted in Fig. 8B for Model 1. Here, the values obtained at different times after starting release (solid symbols) are compared with the theoretical K_a at these times (rightmost values). With fast release the absolute values of the K_a are underestimated. For instance, at $t = 5$ s and $t_{1/2} = 0.3$ s, the apparent calcium sensitivity of release activation is 0.3 μM only, but the correlation between the estimated and theoretically predicted K_a values is still very good ($r = 0.96$; not shown). The contribution of the vesicle depletion error to the shift in the estimated K_a can be judged from the plot of the estimated K_a values at different times as a function of $t_{1/2}$, using Model 2, in which the value of true K_a is constant ($K_a = 2.4$ μM). The results are plotted as open symbols in Fig. 8B. It can be seen that the best results are obtained if the optimal $t_{1/2}$ is more than four times the time constant of the K_a change (which is 1 s in this case). However, the analysis can still be performed without a considerable systematic error when the rates of both processes are similar. In that case, only data for times t shorter than twice the fastest release half time should be analyzed.

The time dependence of apparent K_a, determined from the release curves under different conditions is illustrated in Fig. 9 for Model 1. Fig. 9 shows the apparent K_a values determined with different loading levels, with the approximation of infinite extravesic-

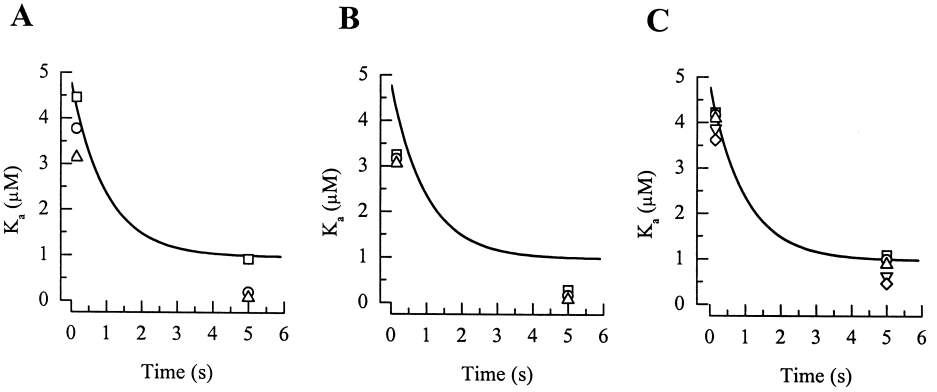

Fig. 9. The apparent K_{Ca} at different times for Model 1 under different conditions of the experiment. The theoretical time course of K_{Ca} is plotted as line. (A) Approximation of infinite extravesicular Ca^{2+} sink. RyR density 1 nmol/l SR. Intravesicular Ca^{2+} (mM): 20 (squares); 2.0 (circles); 0.2 (up triangles). (B) The effect of low extravesicular sink (250 μM EGTA, vesicle dilution 1:50). RyR density 1 nmol/l SR. Intravesicular Ca^{2+} (mM): 20 (squares); 2.0 (circles); 0.2 (up triangles). (C) The effect of RyR density. Approximation of infinite extravesicular sink. Intravesicular $^{45}Ca^{2+}$ 2 mM. RyR density (nmol/l SR): 0.05 (squares); 0.1 (circles); 0.2 (up triangles); 0.5 (down triangles); 1.0 (diamonds).

ular sink (Fig. 9A), and under conditions of low extravesicular Ca^{2+} buffering (250 μM EGTA, vesicle dilution 1:50; Fig. 9B). The effect of RyRC density on the apparent value of K_a is shown in Fig. 9C. It can be seen that low $^{45}Ca^{2+}$ loading and low buffering capacity of the extravesicular medium can distort the values of K_a, but the differences between the initial and steady-state values are not impaired. Increase in receptor density also decreases the apparent values of K_a without changing the difference between initial and steady-state values appreciably.

The sensitivity of the apparent K_a values of Model 3 to receptor density under similar conditions is shown in Fig. 10. It can be seen that this model is much more sensitive to receptor density (Fig. 10A). This sensitivity is decreased if higher total intravesicular calcium concentrations are used (Fig. 10B). The sensitivity of the model is decreased also in the presence of calsequestrin, because the release is slowed down as the free intravesicular Ca^{2+} is decreased, and at the same time, calsequestrin serves as a Ca^{2+} buffer.

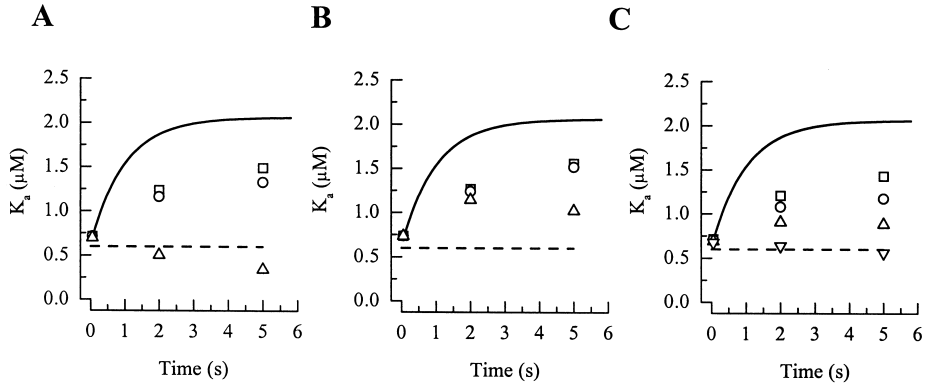

Fig. 10. The apparent K_{Ca} at different times for Model 3 under different conditions of the experiment. The theoretical time course of K_{Ca} is plotted as line. The initial value of K_{Ca} is plotted as dashed line. Approximation of infinite extravesicular Ca^{2+} sink. (A) Control conditions. Intravesicular $^{45}Ca^{2+}$ 2 mM. RyR density (nmol/l SR): 0.01 (squares); 0.1 (circles); 1.0 (up triangles). (B) Effect of increasing intravesicular Ca^{2+}. Intravesicular $^{45}Ca^{2+}$ 2 mM; total intravesicular Ca^{2+} 20 mM. RyR density (nmol/l SR): 0.01 (squares); 0.1 (circles); 1.0 (up triangles). (C) Effect of the presence of calsequestrin. Intravesicular $^{45}Ca^{2+}$ 2 mM. 10 mM Ca^{2+} binding calsequestrin sites. Relative RyR density: 0.03 (squares); 0.3 (circles); 1.0 (up triangles); 3.0 (down triangles).

4. Discussion

The main finding of this work is that the presented complex model of the release experiments, derived solely from the single-channel characteristics of the ryanodine receptor channel, is able to reproduce the calcium dependence of calcium release observed in isolated vesicles of SR. In other words, the model that does not include calcium-dependent inactivation of the channel provides a calcium-dependent decline of the release in the millimolar range of calcium. Previously, decline of the release has been interpreted as reflection of a decrease in channel P_o due to calcium-dependent inactivation [8,13]. However, it is obvious from Figs. 2 and 4 that the simulated release rate declines in the same Ca^{2+} concentration range as was observed experimentally (with the exception of [9]), whereas for the same model the P_o does not decline. It can be concluded that the reported decline of the release rate in the release experiments at millimolar calcium concentrations cannot be regarded any more as a proof of the calcium-dependent inactivation of the cardiac RyR channel.

Extrapolation of these results to the in situ conditions is not possible at present. Any progress in this direction will need a gating model for the RyRC activity in the presence of physiological modulators, such as ATP and Mg^{2+}, including regulation by luminal calcium [33–35]. In the report of Fabiato [1], the decrease of Ca^{2+}-induced Ca^{2+} release was observed at calcium concentrations $\leq$10 μM. This cannot be achieved by the mechanism prominent in the release experiments, i.e. by the decrease in calcium flux through the open pore. From the data in planar lipid bilayers, it seems possible that under physiological concentrations of ATP and at low luminal Ca^{2+}, a low-affinity calcium inactivation site is operating with a K_d between 0.1–0.5 mM [36]. However, this value is still larger than the value observed by Fabiato [1].

Another important outcome of this work is a new method which can be used to resolve the dispute on changes of the RyR channel affinity to calcium following activation [15–18,22–25]. We have found that any changes in channel affinity, if present, are reflected in the release curves, and can be quantitatively evaluated. The described method of analysis has the potential to confirm or refute authenticity of the shift of channel K_a during adaptation [15]. The only condition is to use fast techniques, such as the rapid filtration, quenched flow, or stopped-flow in SR vesicle experiments. However, the application field of the method is more general. It might be useful to quantify the temporal changes in the sensitivity of any channel to agonists. Hot candidates are all channels that control the release of calcium from intracellular stores. In the case of the inositol trisphosphate receptor channel, such an analysis might be useful for understanding of the increment detection phenomenon and its modulation.

The analysis of the effects of experimental conditions and methods of analysis on the observed calcium dependence of release enabled us to pinpoint several factors, listed below, which might have pronounced effects on the results.

(1) The effect of vesicle depletion on the calcium dependence of release activation. Due to the presence of a calcium binding site in the channel pore, the open channel flux is not proportional to the intravesicular $^{45}Ca^{2+}$ concentration. Rather, it is independent of the intravesicular $^{45}Ca^{2+}$ for concentrations above $\sim$100 μM. Therefore, during the time course of release the rate of decline of ^{45}Ca efflux depends on the rate of release in a more complex fashion than it would, had the flux been governed by diffusion. This effect is the most pronounced at the rising part of the calcium dependence curve. It results in shifting the relative release rate curve to the left with respect to the true initial release rate curve, when the initial release rate or cumulative Ca release per time unit are used as the measure of release. The effect is most critical when some or any combination of the following factors occurs: high receptor density, high open probability, low sampling rate, leaky vesicles, low ^{45}Ca loading.

(2) The effect of $^{45}Ca^{2+}$ loading on the calcium dependence of release inhibition. In addition to the effect mentioned above, calcium concentration in the vesicles, via competition between intra- and extravesicular calcium for the binding site in the channel pore, shifts the descending part of the curve to the right when the loading is increased, and to the left when it is decreased. This effect is relatively independent of other experimental conditions and the method of analysis.

(3) The effect of limited extravesicular calcium

buffering capacity (non-infinite extravesicular sink). Increase of the extravesicular Ca^{2+} concentration during the time course of release results in excess activation of the release. Another consequence is dissipation of the ^{45}Ca gradient across the vesicle membrane. The magnitude of this effect is most pronounced at about threshold concentrations of activating calcium. The effect is most critical when low Ca^{2+} buffering capacity (low EGTA concentration or low pH), and/or low dilution of vesicles occurs.

(4) The method of release rate determination. The K_a estimated by the reciprocal half-time method approaches the theoretical value with decreasing Ca^{2+} loading, while for the other two methods it does so with increasing Ca^{2+} loading. The reciprocal half-time method, although having the least demand on $^{45}Ca^{2+}$, has two drawbacks: (a) the descending arm of the calcium dependence is always shifted to the left, giving a K_i value $\sim 50\%$ lower than the true value; and (b) the time dependence of the K_a shifts cannot be evaluated. Therefore the method of choice is the initial rate method.

To assess possible contributions of the low-affinity, inactivating Ca^{2+} binding site proposed by Laver et al. [13] to the decline of Ca^{2+} release rate at high Ca^{2+} concentrations, we have performed the calculations also for a model which includes this low-affinity site (not shown). As expected, the differences from the model having only a single calcium binding site start to be apparent only at the highest Ca^{2+} concentrations. The relative release rate at 15 mM Ca^{2+} decreased from 0.05 in the absence to 0.025 in the presence of the inactivating site, an effect hardly seen in the release experiments. Explanation of the calcium flux 'inactivation' therefore does not necessarily require any distinct calcium-dependent inactivated state of the RyRC. The difference in the open channel flux can be the sole reason for the decline of the release rate under the ionic conditions used for passive release experiments. The inhibition of open probability of the RyRC by Ca^{2+} was detectable in the theoretical release curves, if it occurred at concentrations that did not affect Ca^{2+} flux significantly (data not shown). Such a high tendency for inhibition was observed in the presence of Mg^{2+} and ATP [36]. However, there are no available experimental release data under comparable conditions.

It has been pointed out that a decrease in calcium efflux with increasing extravesicular Ca^{2+} might occur due to a decreased calcium gradient across the SR membrane [37]. With $^{45}Ca^{2+}$ measurements specifically, however, increasing the extravesicular Ca^{2+} concentration does not affect the gradient for $^{45}Ca^{2+}$. Therefore, without the presence of calcium binding sites in the channel pore, i.e. if the flux through the open channel is governed solely by diffusion, the $^{45}Ca^{2+}$ efflux is independent of extravesicular (unlabeled) calcium concentration. The inhibition of $^{45}Ca^{2+}$ efflux through the channel pore by extravesicular calcium, according to the presented model, is explained solely by the competition between intravesicular $^{45}Ca^{2+}$ and extravesicular unlabeled Ca^{2+} for binding to the channel pore. Decreasing capacity of the extravesicular sink cannot significantly influence the concentration dependence of this inhibition.

This is, to our knowledge, the first report in which an explicit gating scheme and permeation model is used to reconstruct the time course of calcium release from the vesicles of cardiac sarcoplasmic reticulum. The time course of Ca^{2+} release from skeletal SR was modeled previously [38] using the approximation of diffusion-limited flux through the channel pore. Our results clearly demonstrate a large impact of the permeation properties of the channel on the time course and on the calcium dependence of release. We conclude that the planar lipid bilayer method can be viewed as a model of choice for studies on the ryanodine receptor channel, as its native properties are preserved after reconstruction to the same extent as in the isolated vesicles. On the other hand, the vesicle release experiments can be an invaluable tool for kinetic studies if conditions of experiment defined in this work are met. These conclusions are important for the design of future experiments, in which the single-channel and flux data may complement each other.

Acknowledgements

A.Z. was supported in part by an International Research Scholar's award from the Howard Hughes Medical Institute and by Grant VEGA 5155, and I.Z. by Grant VEGA 5156. We are grateful to K. Ondriaš and S. Györke for helpful comments on an earlier version of the manuscript.

References

[1] A. Fabiato, Time and calcium dependence of activation and inactivation of calcium-induced calcium release of calcium from the sarcoplasmic reticulum of a skinned canine cardiac Purkinje cell, J. Gen. Physiol. 85 (1985) 247–289.

[2] J.S.K. Sham, L. Cleemann, M. Morad, Functional coupling of Ca^{2+} channels and ryanodine receptors in cardiac myocytes, Proc. Natl. Acad. Sci. USA 92 (1995) 121–125.

[3] J.R. López-López, P.S. Shacklock, C.W. Balke, W.G. Wier, Local calcium transients triggered by single L-type calcium channel currents in cardiac cells, Science 268 (1995) 1042–1045.

[4] M.B. Cannell, H. Cheng, W.J. Lederer, The control of calcium release in heart muscle, Science 268 (1995) 1045–1049.

[5] B.K. Chamberlain, P. Volpe, S. Fleischer, Calcium-induced calcium release from purified cardiac sarcoplasmic reticulum vesicles, J. Biol. Chem. 259 (1984) 7540–7546.

[6] E. Rousseau, J.S. Smith, J.S. Henderson, G. Meissner, Single channel and $^{45}Ca^{2+}$ flux measurements of the cardiac sarcoplasmic reticulum calcium channel, Biophys. J. 50 (1986) 1009–1014.

[7] G. Meissner, J. Henderson, Rapid calcium release from cardiac sarcoplasmic reticulum vesicles is dependent on Ca^{2+} and is modulated by Mg^{2+}, adenine nucleotide, and calmodulin, J. Biol. Chem. 262 (1987) 3065–3073.

[8] A. Chu, M. Fill, E. Stefani, M.L. Entmann, Cytoplasmic Ca^{2+} does not inhibit the cardiac muscle sarcoplasmic reticulum ryanodine receptor Ca^{2+} channel, although Ca^{2+}-induced Ca^{2+} inactivation of Ca^{2+} release is observed in native vesicles, J. Membr. Biol. 135 (1993) 49–59.

[9] L.G. Mészáros, J. Bak, A. Chu, Cyclic ADP-ribose as an endogenous regulator of the non-skeletal type ryanodine receptor Ca^{2+} channel, Nature 364 (1993) 76–79.

[10] R.H. Ashley, A.J. Williams, Divalent cation activation and inhibition of single calcium release channels from sheep cardiac sarcoplasmic reticulum, J. Gen. Physiol. 95 (1990) 981–1005.

[11] S. Györke, P. Vélez, B. Suárez-Isla, M. Fill, Activation of single cardiac and skeletal ryanodine receptor channels by flash photolysis of caged Ca^{2+}, Biophys. J. 66 (1994) 1879–1886.

[12] R. Sitsapesan, A.J. Williams, Gating of the native and purified cardiac SR Ca^{2+}-release channel with monovalent cations as permeant species, Biophys. J. 67 (1994) 1484–1494.

[13] D.R. Laver, L.D. Roden, G.P. Ahern, K.R. Eager, P.R. Junankar, A.F. Dulhunty, Cytoplasmic Ca^{2+} inhibits the ryanodine receptor from cardiac muscle, J. Membr. Biol. 147 (1995) 7–22.

[14] A. Zahradníková, I. Zahradník, Description of modal gating of the cardiac calcium release channel in planar lipid membranes, Biophys. J. 69 (1995) 1780–1788.

[15] S. Györke, M. Fill, Ryanodine receptor adaptation: control mechanism of Ca^{2+}-induced Ca^{2+} release in heart, Science 260 (1993) 807–809.

[16] H.H. Valdivia, J.H. Kaplan, G.C.R. Ellies-Davies, W.J. Lederer, Rapid adaptation of cardiac ryanodine receptors: modulation by Mg^{2+} and phosphorylation, Science 267 (1995) 1997–2000.

[17] A. Schiefer, G. Meissner, G. Isenberg, Ca^{2+} activation and Ca^{2+} inactivation of canine reconstituted cardiac sarcoplasmic reticulum Ca^{2+}-release channels, J. Physiol. 489 (1995) 337–348.

[18] R. Sitsapesan, R.A.P. Montgomery, A.J. Williams, New insights into the gating mechanisms of cardiac ryanodine receptors revealed by rapid changes in ligand concentration, Circ. Res. 77 (1995) 765–772.

[19] D.R. Laver, B.A. Curtis, Response of ryanodine receptor channels to Ca^{2+} steps produced by rapid solution changes, Biophys. J. 71 (1996) 732–741.

[20] K. Yasui, P. Palade, S. Györke, Negative control mechanism with features of adaptation controls Ca^{2+} release in cardiac myocytes, Biophys. J. 67 (1994) 457–460.

[21] A. Zahradníková, I. Györke, S. Györke, Modal transitions during calcium release channel adaptation, Biophys. J. 70 (1996) A145.

[22] G.D. Lamb, D.G. Stephenson, Activation of ryanodine receptors by flash photolysis of caged Ca^{2+}, Biophys. J. 68 (1995) 946–948.

[23] H. Cheng, M. Fill, H. Valdivia, W.J. Lederer, Models of Ca^{2+} release channel adaptation, Science 267 (1995) 2009–2010.

[24] M.D. Stern, 'Adaptive' behavior of ligand-gated ion channels: constraints by thermodynamics, Biophys. J. 70 (1996) 2100–2109.

[25] A. Zahradníková, I. Zahradník, A minimal gating model for the cardiac calcium release channel, Biophys. J. 71 (1996) 2996–3012.

[26] A. Tinker, A.R.G. Lindsay, A.J. Williams, A model for ionic conduction in the ryanodine receptor channel of sheep cardiac muscle sarcoplasmic reticulum, J. Gen. Physiol. 100 (1992) 495–517.

[27] K. Cooper, E. Jakobsson, P. Wolynes, The theory of ion transport through membrane channels, Prog. Biophys. Mol. Biol. 46 (1985) 51–96.

[28] P.D. Smith, G.W. Liesegang, R.L. Berger, G. Czerlinski, R.J. Podolsky, A stopped-flow investigation of calcium ion binding by ethylene glycol bis(beta-aminoethyl ether)-N,N′-tetraacetic acid, Anal. Biochem. 143 (1984) 188–195.

[29] G.L. Smith, D.J. Miller, Potentiometric measurements of stoichiometric and apparent affinity constants of EGTA for protons and divalent ions including calcium, Biochim. Biophys. Acta 839 (1985) 287–299.

[30] J. Wagner, J. Keizer, Effects of rapid buffers on Ca^{2+} diffusion and Ca^{2+} oscillations, Biophys. J. 67 (1994) 447–456.

[31] D.M. Bers, Excitation–Contraction Coupling and Cardiac Contractile Force, Kluwer, Boston, 1994.

[32] J. Keizer, L. Levine, Ryanodine receptor adaptation and Ca^{2+}-induced Ca^{2+} release-dependent Ca^{2+} oscillations, Biophys. J. 71 (1996) 3477–3487.

[33] R. Sitsapesan, A.J. Williams, Regulation of the gating of the

sheep cardiac sarcoplasmic reticulum Ca^{2+}-release channel by luminal Ca^{2+}, J. Membr. Biol. 137 (1994) 215–226.
[34] J.W.M. Bassani, W.L. Yuan, D.M. Bers, Fractional SR Ca release is regulated by trigger Ca and SR Ca content in cardiac myocytes, Am. J. Physiol. 37 (1995) C1313–C1319.
[35] V. Lukyanenko, I. Györke, S. Györke, Regulation of calcium release by calcium inside the sarcoplasmic reticulum in ventricular myocytes, Pflügers Arch. 432 (1996) 1047–1054.
[36] I. Györke, S. Györke, Regulation of the cardiac RyR channel by cytoplasmic and lumenal calcium, Biophys. J. 74 (1998) A56.
[37] R. Coronado, J. Morrissette, M. Sukhareva, D.M. Vaughan, Structure and function of ryanodine receptors, Am. J. Physiol. 266 (1994) C1485–C1504.
[38] W. Wyskovsky, M. Hohenegger, B. Plank, G. Hellmann, S. Klein, J. Suko, Activation and inhibition of the calcium-release channel of isolated skeletal muscle heavy sarcoplasmic reticulum, Eur. J. Biochem. 194 (1990) 549–559.